

THE COSMOLOGICAL MEAN DENSITY AND ITS LOCAL VARIATIONS PROBED BY PECULIAR VELOCITIES

ROYA MOHAYAEE¹, R. BRENT TULLY²

Draft version February 7, 2020

ABSTRACT

Peculiar velocities throughout the region of the local supercluster are reconstructed by two different orbit-retracing methods. The requirement of the optimal correlation between the radial components of reconstructed velocities and the observed peculiar velocities derived from our extensive new catalog of distances puts stringent constraints on the values of the cosmological parameters. Our constraints intersect those from studies of microwave background fluctuations and statistical properties of galaxy clustering: the ensemble of constraints are consistent with $\Omega_m = 0.22 \pm 0.02$. While motions throughout the Local Supercluster provide a measure of the mean ratio of mass to light, there can be large local fluctuations. Our reconstruction of the infall velocities in the immediate vicinity of the Virgo Cluster shows that there is a mass-to-light anomaly of a factor of 3 to 6 between groups in the general field environment and the heavily populated Virgo Cluster.

Subject headings: dark matter — cosmological parameters — methods:analytical and numerical

1. INTRODUCTION

Cosmological parameters have been significantly constrained by the combined analyses of the data mainly from Cosmic Microwave Background (CMB) radiation, large-scale galaxy distribution, supernova observations and cosmic shear field [see *e.g.* (Tegmark et al. 2004)]. Here, we demonstrate that analysis of the peculiar velocity field can tighten the constraints on cosmological models because error ellipses are strongly skewed to those of *WMAP* and SDSS in the parameter space of density and age. Two complementary theoretical methods are used in this paper to generate orbits that give velocities to be compared with observations. Peculiar velocities are defined by a high density of quality distance measures. Good distances are available for 1400 galaxies within 3,000 km s⁻¹.

The two variational methods used here are based on the principle that galaxies as mass-tracers follow orbits which are the stationary points of the Euler-Lagrange action. Our first approach, the *Least Action* (LA) method (Peebles 1989), can provide descriptions of orbits in the nonlinear collapse regime, though recovered trajectories are non-unique due to lack of knowledge of the initial positions of galaxies and because of orbit-crossing (*i.e.* multistreaming). Yet, although there are limitations on the orbit specifics, accurate distance estimates provide tight limits on the mass distribution in reasonable models through constraints on the end points of orbits. On large scales, a unique reconstruction is possible since the displacement of dark matter fluid becomes almost potential and multistreaming becomes less severe. These properties are at the basis of our second method, MAK (Frisch et al. 2002), which can be used to uniquely and efficiently construct the peculiar velocity field on large scales.

With both LA and MAK, a reconstructed velocity

field based on a set of cosmological parameters is tested against observed distances and a χ^2 statistic is used to determine the best range of the parameters. Allowing for statistical and systematic errors and considering all the methods in tandem, we show that the MAK, LA, *WMAP* and SDSS results give preference to a small region in parameter space centered at age $t_0 = 13.5$ Gyr and density parameter $\Omega_m = 0.22 \pm 0.02$ at $H_0 = 80$ km s⁻¹ Mpc⁻¹. The low value of Ω_m obtained here is consistent with that found from the cluster mass function (Bahcall et al. 2003) and from some simulations (Ostriker 2003).

The large-scale velocity field analyses begin with the simplistic assumption of constant M/L . However, there is good evidence from galaxy flows near the Virgo Cluster that the situation is more complicated. The high velocities of infall are unmistakable evidence of a large M/L for the cluster. Reconstruction of the amplitude of the first approach infall velocities provides a determination of the mass of the cluster at radii beyond the virialized region; radii greater than those explored by X-ray or lensing studies or by studies of the motions of galaxies within the cluster. We show that the high amplitude observed in the infall region requires an assignment of $M/L = 500M_\odot/L_\odot$ to the Virgo Cluster, significantly higher than the value associated with the spiral-dominated field (usually 100-200 M_\odot/L_\odot).

2. CATALOG OF NEARBY GALAXIES AND DISTANCES

The catalog of galaxies, is a 40% augmentation of the Nearby Galaxies Catalog (Tully 1987), now including 3300 galaxies within 3,000 km s⁻¹. This depth is more than twice the distance of the dominant component, the Virgo Cluster, and the completion to this depth in the current catalog compares favorably with other all-sky surveys [*e.g.*, 2MASS (Jarrett 2004)]. The catalog has the following properties. (i) All entries are given a detailed group and filament assignment (or non-assignment if isolated). (ii) The catalog is supplemented by an all-sky complete sample of X-ray selected clusters (Kocevski et al. 2004) in the shell 3,000–8,000 km s⁻¹ to provide a description of potential influences on very large scales.

¹ Institut d’astrophysique de Paris, 98bis bd Arago, 75014 Paris, France

² Institute for Astronomy, University of Hawaii, Honolulu, HI 96822, USA

(iii) ‘Fake’ galaxies are added at low Galactic latitudes to avoid an underdensity in the zone of obscuration due to lost information. (iv) Correction is made for the loss of light with distance caused by an apparent magnitude cutoff in the construction of the catalog.

The second observational component is an extended catalog of galaxy distances. Information from four techniques has been integrated: the Cepheid variable (Freedman et al. 2001), Tip of the Red Giant Branch (Karachentsev 2003; Lee et al. 1993), Surface Brightness Fluctuation (Tonry & Schneider 1988; Tonry et al. 2001), and Luminosity–Linewidth (Tully & Fisher 1977; Tully & Pearce 2000) methods. In all, there are over 1400 galaxies with distance measures within the $3,000 \text{ km s}^{-1}$ volume; over 400 of these are derived by at least one of the first three ‘high quality’ techniques. In the present study, distances are averaged over groups because orbits cannot meaningfully be recovered on sub-group scales. The present catalog is assembled into 1234 groups (including groups of one) of which 633 have measured distances. These observational components will be described in detail in a later publication.

3. TECHNIQUES: THE LA AND MAK METHODS

Peebles pioneered the Least Action method (Peebles 1989, 1994, 1995) that requires orbits to satisfy the stationary point of the Euler-Lagrange action, the integral over time of the Lagrangian. Hence, least action searches for the minimum of

$$S_{\text{LA}} = \int_0^{t_0} dt \left[\frac{m_i a^2 \dot{\mathbf{x}}_i^2}{2} - \frac{G m_i m_j}{a |\mathbf{x}_i - \mathbf{x}_j|} + \frac{2}{3} \pi G \rho_b a^2 m_i \mathbf{x}_i^2 \right], \quad (1)$$

where summation over repeated indices and $j \neq i$ is implied, t_0 denotes the present time, the path of the i th particle with mass m_i is $\mathbf{x}_i(t)$, ρ_b is the mean mass density, and the present value of the expansion parameter $a(t)$ is $a_0 = a(t_0) = 1$.

Individual orbits are constrained by the mixed boundary conditions that peculiar velocities were initially negligible (they subsequently grew from gravitational perturbations) and the known elements of position and velocity today. The other piece of information known for roughly half the elements is the aforementioned distances. This information is used to discriminate between models. A given model involves a specification of cosmological parameters and the assignment of mass to each of the elements. Orbita are found within the context of a specified model that are consistent with the boundary condition constraints on angular positions and radial velocities. A component of the end point of an orbit is its distance which can be compared with the observed distance. Different models result in different distances. The quality of a model can be evaluated by a statistical measure of the differences between observed and model distance moduli, μ_{obs} and μ_{mod} respectively. A χ^2 parameter can be calculated for each element, i , with a measured distance, $\chi_i^2 = (\mu_{\text{mod},i} - \mu_{\text{obs},i})^2 / \epsilon_i^2$, where ϵ_i is the uncertainty assigned to $\mu_{\text{obs},i}$. A comparison of the relative distribution of χ_i^2 values provides a sensitive discriminant between good and bad models (Shaya et al. 1995; Phelps 2002).

Galaxy flows are not sensitive to any uniform repulsive dark energy (Lahav et al. 1991; Shaya et al. 1995). Mea-

surements of the lowest frequency peak in the microwave background fluctuation spectrum strongly indicate, and we accept, that the Universe has a flat topology, whence $\Omega_\Lambda + \Omega_m = 1$ where Ω_Λ characterizes the mean density of dark energy and Ω_m characterizes the mean density of matter with respect to the critical density for a flat Universe in matter alone. Specification of Ω_m and the Hubble Constant, H_0 , which describes the mean expansion rate of the Universe, in the context of a flat Universe uniquely specifies the age of the Universe, $t_0(\Omega_m, H_0)$.

The Least Action orbits are a reflection of the interactions of masses over the age of the Universe. As an initial approximation, it is assumed that the relationship between mass and light is constant so the mass M_i assigned to an element in the catalog with luminosity L_i is $M_i = (M/L)L_i$. Consequently, a cosmological model to be explored is specified by two fundamental parameters: $t_0(\Omega_m, H_0)$ and M/L . For a given choice of t_0 and M/L , orbits are constructed, model distances at the end points are determined and compared with observed distances, and the match provides a χ^2 measure that can be compared with alternative models. Discrimination between results over the domain of $(t_0, M/L)$ choices based on the χ^2 measure gives specification of a best model.

The alternate technique that will be implemented here is the Monge-Ampère-Kantorovich (MAK) reconstruction (Frisch et al. 2002; Mohayaee et al. 2003; Brenier et al. 2003). This method provides a recipe for the orbits that is unique to the degree that orbits can be described as following straight lines. Orbita in the MAK reconstruction are minima of the action which assume a Lagrangian mapping $\mathbf{q} \mapsto \mathbf{x}$ that can be described in terms of a potential as $\mathbf{x} = \nabla_{\mathbf{q}} \Phi(\mathbf{q})$. Here, \mathbf{x} is the current Eulerian position and \mathbf{q} is the initial Lagrangian position. The potential $\Phi(\mathbf{q})$ is assumed to be convex; ie, orbit-crossing is excluded. With these conditions, orbits are reconstructed uniquely by an assignment algorithm that finds the minimum in the ensemble of orbit distances summed in quadrature. Hence, MAK search for the minimum of the discretized action

$$S_{\text{MAK}} = \min_{j(\cdot)} \left(\sum_{i=1}^N (\mathbf{q}_{j(i)} - \mathbf{x}_i)^2 \right). \quad (2)$$

It is insightful to note that the least action variation (1) reduces to MAK optimization (2) for inertial trajectories.

The distances, d , permit an extraction of peculiar velocities $V_{\text{pec}} = V_{\text{gsr}} - dH_0$ where V_{gsr} is the observed velocity of an object in the galactic standard of rest. The relationship between redshift and real space displacements of the elements is estimated using the approximation that galaxies trace mass on inertial trajectories (Zel'dovich 1970): $\mathbf{v} = f\mathbf{H}(\mathbf{x} - \mathbf{q})$ where \mathbf{v} is the peculiar velocity vector and $f \sim \Omega_m^{0.6}$. Consequently, a specific model defines positions that can be tested against observed positions in the same way that is done in the Least Action analysis.

An advantage of Least Action is that it potentially can be used in the highly non-linear regime where orbits are strongly curved. An advantage of MAK is that it recovers orbits uniquely and quickly, hence can be used with the very large catalogs that are becoming available. By using the two methods on the identical catalogs, with the identical distance constraints, it is affirmed that the

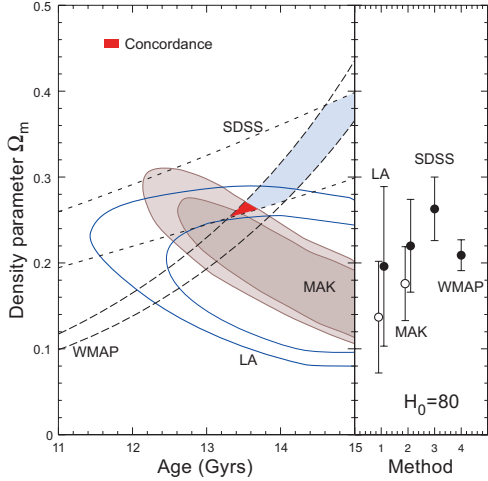


FIG. 1.— Reconstruction methods constrained by precision distance measures give estimates of the mean mass density of the Universe. The contours are χ^2 at 1 and 2σ for models with different choices of age and mass density Ω_m , with shaded contours for MAK and line contours for LA reconstructions. The MAK and Least Action contours are adjusted upward in density by 20% and 30% respectively to compensate for systematic underestimations of density. The confluence of the constraints on density and age parameters from *WMAP* (Spergel 2003) of $\Omega_m h^2 = 0.134$ and from *SDSS* (Tegmark et al. 2004) of $\Omega_m h = 0.21$ is lightly shaded. The darkest shaded region lies within the 2σ limits of all four experiments. The right panel shows the density determinations for LA, MAK, SDSS, and *WMAP* for $H_0 = 80 \text{ km s}^{-1} \text{ Mpc}^{-1}$, the value of the Hubble Constant consistent with our distance scale zero point. The open and filled symbols for LA and MAK respectively give the results before and after compensation for the systematic under-determination of mass density. At $H_0 = 80$, $t_0^{SDSS} = 12.2 \text{ Gyr}$, $t_0^{WMAP} = 13.0 \text{ Gyr}$, and $t_0^{MAK,LA} = 13.5 \text{ Gyr}$. The 4 analyses are consistent with $\Omega_m = 0.22 \pm 0.02$ with the constrained value of H_0 .

two methods recover similar results in the regimes where they are both applicable.

Both methods have been tested on N-body simulations and found to result in modest underestimations of the known densities. Underestimates are anticipated because, at one extreme, mass that is not strongly clustered on the scale of the survey has little dynamical consequence and, at the other extreme, complex shell-crossing orbits cannot be modeled. Analysis of MAK reconstructions in 12 cosmological simulations with different initial fluctuation characteristics discussed by Mohayaee et al. (2005) resulted in recovery of $80\% \pm 20\%$ (1σ) of the known model density. In the case of Least Action, it has been appreciated that mass can be underestimated on small scales (Branchini & Carlberg 1994; Branchini et al. 2002). A quantitative measure of the effect is found using our Least Action reconstruction algorithms with an N-body simulation with $\Omega_\Lambda = 0.7$, $\Omega_m = 0.3$, evaluated by placing the observer at multiple locations to test for cosmic variance. Recovered densities were $70\% \pm 20\%$ of the model density (Phelps, Desjacques, and Nusser; ongoing work).

4. RESULTS: I. DETERMINATION OF Ω_m

The results of the two methods are summarized in Fig. 1 where contours of the χ^2 parameter are plotted in the domain $\{t_0, \Omega_m\}$. In the case of the Least Action

analysis, mass density Ω_m is derived from M/L values by accepting the mean B band luminosity density of the Universe determined from SDSS Blanton et al. (2003) with reddening corrections. We use $M/L = \Omega_m 1540h$, a transform with $\sim 20\%$ uncertainty.

The error ellipses from the MAK and LA studies are elongated. With a linear analysis the elliptical χ^2 troughs would open to infinity, but non-linear effects create a specific minimum along each χ^2 trough. At a fixed age, t_0 , there are relatively tight constraints on Ω_m requirements. If shorter ages are entertained, then higher densities are required to arrive at the observed dynamical state in the specified time. The contrary dependence between density and time are seen in the results from the microwave background *WMAP* (Spergel 2003) and galaxy redshift *SDSS* (Tegmark et al. 2004) experiments that are also superimposed on Fig. 1. Only a small domain around $t_0 = 13.5$ Gyr lies within or near the 2σ contours of all the methodologies. With the constraint $h = 0.8$ consistent with the zero point of the distance estimates, there is good agreement between the *WMAP*, *SDSS*, MAK, and LA measures of the density parameter: $\Omega_m = 0.22 \pm 0.02$.

5. RESULTS: II. THE MASS OF VIRGO CLUSTER

The velocity field analyses discussed above make the simplistic assumption of constant M/L . There is good evidence from galaxy flows near the Virgo Cluster that the situation is more complicated. The high velocities of infall suggest a large M/L for the cluster. The critical galaxies for this discussion lie outside the cluster on the plane of the sky so only a modest component of the infall motion is projected into the line of sight but there is no confusion with cluster membership. Galaxies infalling from the foreground of the cluster are redshifted with respect to the cluster and galaxies infalling from the background are blueshifted. If one could imagine many test particles distributed along a line of sight, they would create a wave in velocity as a function of distance with the same velocity arising at three distances (Tonry & Davis 1981) – two located within the infall region and one located at the cosmic expansion position. The amplitude of the peaks of the ‘triple-value’ waves depend on the mass, M , interior to the position associated with the peaks, r . The envelope of observed infall velocities with r provides a description (Tully & Shaya 1984) of the run of $M(< r)$. The outermost caustic of the Virgo Cluster proper (the radius of second turnaround) is at ~ 2 Mpc from the center of the cluster. Galaxies on first infall acquire very high radial velocities at 2–4 Mpc from the Virgo core.

An example is given in Fig. 2. The run of velocities with distance are what is expected along the specific line of sight of the 11–3 group in the Nearby Galaxies Catalog with three different assumptions regarding the mass of the Virgo Cluster. The observed distance and velocity of the 11–3 group is indicated in the figure. It is clear that the 11–3 group is at one of the two infall locations (or the location where the two infall positions become degenerate at the tip of the triple-value curve) rather than at the cosmic expansion position around 30 Mpc.

The total mass within $3,000 \text{ km s}^{-1}$ is the same in all 3 models to ensure that the global χ^2 is near the minimum of the trough in Fig. 1, however the distribution of mass between the elliptical rich and spiral rich groups is

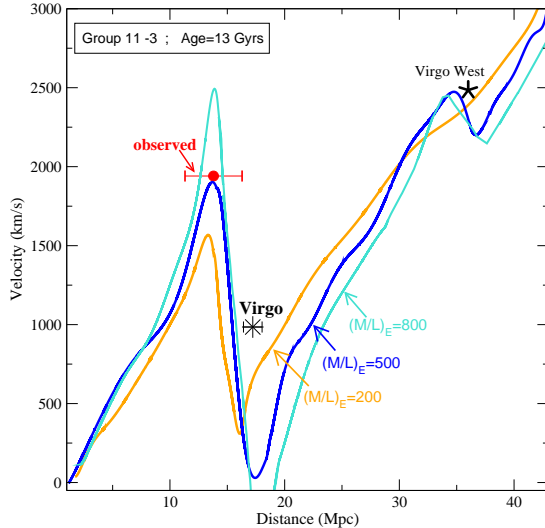


FIG. 2.— The distortion of the velocity–distance relation by the Virgo Cluster in the line of sight toward the 11–3 group. The observed distance and velocity of the 11–3 group is indicated by the point with error bars in distance (errors in velocity are smaller than the symbol). The observed distance and velocity of the Virgo Cluster is indicated (centered at 6.2 degrees from the line of sight of the 11–3 group). The background Virgo W Cluster causes the second wiggle along this line of sight. The behaviour of infall into the Virgo Cluster is traced by the locus of positions and velocities of test particles of negligible mass that were laid down in the line of sight of the 11–3 group and subjected to Least Action modeling. It is concluded from the information seen on this plot and equivalent plots of the lines of sight to other groups close to the Virgo Cluster that $M/L_{\text{Virgo}} \approx 500M_{\odot}/L_{\odot}$ and the mean M/L for the field outside the cluster is approximately 1/3 of this value.

modified between models. Here, $t_0 = 13$ Gyr. In the case of the curve with the smallest swing, all components are given the same $M/L = 200M_{\odot}/L_{\odot}$. The intermediate curve is generated with the elliptical-dominated groups (including the Virgo Cluster) given $M/L_E = 500$ and the spiral-dominated groups given $M/L_S = 174$. The curve with the largest swing reflects $M/L_E = 800$ and $M/L_S = 148$. In the model illustrated by the middle curve in Fig. 2, the cluster is given the necessary and just sufficient mass of $9 \times 10^{14}M_{\odot}$.

The 11–3 group and a couple of others provide the greatest demands on the mass of the cluster and are inferred to lie near a tip along a triple-value curve. An

adequate description of the amplitude of their infall velocities requires an assignment of $M/L = 500M_{\odot}/L_{\odot}$ to the Virgo Cluster if $t_0 = 13$ Gyr. As with the overall supercluster modeling, less cluster mass is required if given more time (Tully & Shaya 1984): *e.g.*, $8 \times 10^{14}M_{\odot}$ suffices if $t_0 = 14$ Gyr. In both these 13 and 14 Gyr cases, as the mass assigned to the cluster is augmented, the models require a reduction of mass assigned to the field to remain at the minimum of the χ^2 trough of Fig. 1. The ratio of cluster, C , to field, F , mass to light values is $(M/L)_C/(M/L)_F \simeq 3$ with the mass assignments required to explain the infall motions. This factor 3 probably underestimates the M/L difference between Virgo and bound groups in the field because some of the mass contributing to the field ratio lies outside the groups. Studies of the dynamics of nearby groups (Tully 2005) suggest that bound groups of spiral galaxies in the field have $M/L \sim 90$. The mass to light ratio of the Virgo Cluster is 5–6 times larger.

6. CONCLUSIONS

Our first result on the mean density of the Universe complements the *WMAP* and SDSS measurements of the density parameter because the error ellipses in the domain Ω_m, H_0 are steeply inclined to each other. A narrow range of parameter space around $t_0 = 13.5$ Gyr, $\Omega_m = 0.22 \pm 0.02$ is permitted by the combined experiments.

Our second result concerns the local fluctuations around this mean density. Although most of the blue light in the local Universe is associated with the spiral field, there is close to parity in the partition of mass between the spiral field and the Virgo Cluster. The M/L value associated with the E/S0 dominated Virgo Cluster is significantly higher than that associated with the spiral dominated field.

We thank Ed. Bertschinger, J. Colin, U. Frisch, M. Hénon, G. Lavaux, P.J.E. Peebles, S. Phelps, E. Shaya and J. Silk for discussions, collaboration and support. RM was supported by a Marie Curie fellowship. RBT acknowledges support from the BQR program of the Observatoire de la Côte d’Azur, the French Hautes Niveaux of EGIDE, a JPL Space Interferometry Mission contract, and STScI and NSF awards.

REFERENCES

Bahcall, N.A. et al., *ApJ*, **585**, 182–190 (2003).
 Blanton, M.R., et al. *Astrophys. J.* **592**, 819–838 (2003).
 Branchini, E. & Carlberg, R.G. *Astrophys. J.* **434**, 37–45 (1994).
 Branchini, E., Eldar, A. & Nusser, A. *MNRAS* **335**, 53–72 (2002).
 Brenier, Y., Frisch, U., Hénon, M., Loepfer, S., Matarrese, S., Mohayaee, R., & Sobolevskii, A. *Mon. Not. R. Astron. Soc.* **346**, 501–524 (2003).
 Freedman, W.L., et al. *Astrophys. J.* **553**, 47–72 (2001).
 Frisch, U., Matarrese, S., Mohayaee, R. & Sobolevskii, A. *Nature*, **417**, 260–262 (2002).
 Jarrett, T.H. *Publ. Astron. Soc. Australia*, **21**, 396–403 (2004).
 Karachentsev, I.D., et al. *Astron. Astrophys.*, **398**, 479–491 (2003).
 Kocevski, D.D., Mullis, C.R. & Ebeling, H. *Astrophys. J.* **608**, 721–730 (2004).
 Lahav, O., Lilje, P.B., Primack, J.R., & Rees, M.J. *Mon. Not. R. Astron. Soc.* **251**, 128–136 (1991).
 Lee, M.G., Freedman, W.L. & Madore, B.F. *Astrophys. J.* **417**, 553–559 (1993).
 Mohayaee, R., Frisch, U., Matarrese, S. & Sobolevskii, A. *Astron. Astrophys.*, **406**, 393–401 (2003).
 Mohayaee, R., Mathis, H., Colombi, S. & Silk, J. *astro-ph/0501217*.
 Ostriker, J.P., Nagamine, K., Cen, R. & Masataka, F., *ApJ*, **597**, 1–8 (2003).
 Peebles, P.J.E. *Astrophys. J.* **344**, L53–L56 (1989).
 Peebles, P.J.E. *Astrophys. J.* **429**, 43–65 (1994).
 Peebles, P.J.E. *Astrophys. J.* **449**, 52–60 (1995).
 Phelps, S.D. *Astrophys. J.* **575**, 1–6 (2002).
 Shaya, E.J., Peebles, P.J.E., & Tully, R.B. *Astrophys. J.* **454**, 15–31 (1995).
 Spergel, D.N., et al. *Astrophys. J. Suppl.* **148**, 175–194 (2003).
 Tegmark, M., et al. *Phys. Rev. D*, **69**, 103501–103527 (2004).
 Tonry, J.L. & Davis, M. *Astrophys. J.* **246**, 680–695 (1981).
 Tonry, J.L. & Schneider, D.P. *Astron. J.* **96**, 807–815 (1988).
 Tonry, J.L., Dressler, A., Blakeslee, J.P., Ajhar, E.A., Fletcher, A.B., Luppino, G.A., Metzger, M.R. & Moore, C.B. *Astrophys. J.* **546**, 681–693 (2001).

Tully, R.B. & Fisher, J.R. *Astron. Astrophys.*, **54**, 661–673 (1977).
Tully, R.B. & Pierce, M.J. *Astrophys. J.* **533**, 744–780 (2000).
Tully, R.B. & Shaya, E.J. *Astrophys. J.* **281**, 31–55 (1984).
Tully, R.B. *Nearby Galaxies Catalog*, Camb. Univ. Press (1987).
Tully, R.B. *Astrophys. J.* **618**, 214–226 (2005).
Zel'dovich, Ya.B. *Astron. & Astrophys.* **5**, 84–89 (1970).